THE JOURNAL OF COMPARATIVE NEUROLOGY 489:293–310 (2005)

Diversity of Ganglion Cells in the Mouse Retina: Unsupervised Morphological Classification and Its Limits

JEE-HYUN KONG, DANIEL R. FISH, REBECCA L. ROCKHILL, AND RICHARD H. MASLAND*
Howard Hughes Medical Institute, Massachusetts General Hospital, Harvard Medical School, Boston, Massachusetts 02114

ABSTRACT

The dendritic structures of retinal ganglion cells in the mouse retina were visualized by particle-mediated transfer of DiI, microinjection of Lucifer yellow, or visualization of green fluorescent protein expressed in a transgenic strain. The cells were imaged in three dimensions and the morphologies of a series of 219 cells were analyzed quantitatively. A total of 26 parameters were studied and automated cluster analysis was carried out using the k-means methods. An effective clustering, judged by silhouette analysis, was achieved using three parameters: level of stratification, extent of the dendritic field, and density of branching. An 11-cluster solution is illustrated. The cells within each cluster are visibly similar along morphological dimensions other than those used statistically to form the clusters. They could often be matched to ganglion cell types defined by previous studies. For reasons that are discussed, however, this classification must remain provisional. Some steps toward more definitive methods of unsupervised classification are pointed out. J. Comp. Neurol. 489: 293–310, 2005.

Indexing terms: regina; ganglion cell; type; mouse

As was recognized by Cajal, the central issue for a bottom-up understanding of complex neural systems is to identify the functional types of neuron. These are the essential building blocks upon which all neural computations are based. Ultimately, this identification will probably be made on the basis of molecular markers of neuronal types. However, markers specific to individual neuronal cell types in most CNS circuits have not been forthcoming. Although specialized cells (viz., rod and cone photoreceptors) have unique proteins, and large classes of neurons (viz., amacrine cells) share certain molecules, at the level of functional cell types only a few cell-type-specific proteins are known and these typically turn out to be only partially specific, i.e., to be shared among several neuronal types (Gustincich et al., 1997, 1999; review, Masland and Raviola, 2000). Developmental specificity instead appears to be combinatorial, with developmental time as one of the parameters.

Until it is learned how to use this specificity to generate markers that can be expressed in adult animals, the most general method remains neuronal morphology. Morphology serves as a neuronal signature, allowing one type to be distinguished from another. It also has the advantage that it is a powerful step toward knowledge of connectivity. The shapes of neurons are caused by the trajectories of axons and dendrites as they make their connections with other cells. Thus, shape is both an identifier and an initial blueprint to the cell's wiring.

Historically, cell shape has been distinguished by a combination of various features, sometimes explicitly stated but more often only partly so. In more formal terms, anatomists since Cajal have made classifications of cells in multiparameter spaces. As will be discussed in more detail below, the problem resembles some aspects of face recognition—how one can distinguish among the thousands of individual humans that one easily recognizes

This article includes Supplementary Material available via the internet at http://www.interscience.wiley.com/jpages/0021-9967/suppmat.

The first two authors contributed equally to this work.

*Correspondence to: Richard H. Masland, Massachusetts General Hospital, 50 Blossom St., Wellman 429, Boston, MA 02114.
E-mail: masland@helix.mgh.harvard.edu

Received 30 December 2004; Revised 10 March 2005; Accepted 20 March 2005

DOI 10.1002/cne.20631

Published online in Wiley InterScience (www.interscience.wiley.com).

TABLE 1. Correlations among 26 Morphological Parameters

	1	2	3	4	5	6	7	8	9	10	11	12	13	14	15	16	17	18	19	20	21	22	23	24	25	26
1	1.00	0.16	0.03	0.07	−0.17	−0.16	−0.74	−0.75	−0.73	−0.65	0.75	0.79	0.79	0.74	0.50	0.79	0.27	0.27	−0.09	−0.09	−0.23	−0.16	−0.46	−0.30	−0.45	−0.40
2	0.16	1.00	−0.27	0.48	0.01	−0.22	−0.22	−0.33	−0.33	−0.28	−0.10	0.16	−0.08	0.16	−0.10	0.15	0.07	0.07	0.08	0.02	−0.19	−0.17	−0.01	−0.02	−0.08	−0.04
3	0.03	−0.27	1.00	−0.25	−0.03	0.33	0.14	0.25	0.20	0.29	0.30	−0.09	0.22	−0.11	0.33	−0.01	−0.19	−0.19	0.06	0.03	0.21	0.10	0.15	0.06	0.23	0.01
4	0.07	0.48	−0.25	1.00	0.03	−0.18	−0.12	−0.20	−0.15	−0.22	−0.11	0.09	−0.06	0.10	−0.15	0.04	0.12	0.14	0.04	0.06	−0.06	0.04	−0.05	0.06	−0.19	0.02
5	−0.17	0.01	−0.03	0.03	1.00	0.16	0.22	0.17	0.07	0.29	−0.07	−0.16	−0.18	−0.20	0.11	0.00	−0.28	−0.26	0.00	−0.03	0.05	0.02	0.11	0.15	0.05	0.10
6	−0.16	−0.22	0.33	−0.18	0.16	1.00	0.59	0.53	0.36	0.68	0.35	−0.59	0.12	−0.60	0.63	−0.43	−0.58	−0.53	−0.14	−0.02	0.45	0.30	0.49	0.31	0.47	0.20
7	−0.74	−0.22	0.14	−0.12	0.22	0.59	1.00	0.89	0.77	0.90	−0.39	−0.77	−0.51	−0.74	−0.10	−0.73	−0.45	−0.43	−0.03	0.02	0.37	0.25	0.53	0.34	0.53	0.40
8	−0.75	−0.33	0.25	−0.20	0.17	0.53	0.89	1.00	0.95	0.89	−0.25	−0.70	−0.33	−0.66	−0.06	−0.69	−0.32	−0.30	0.07	0.08	0.38	0.29	0.41	0.28	0.42	0.34
9	−0.73	−0.33	0.20	−0.15	0.07	0.36	0.77	0.95	1.00	0.71	−0.27	−0.59	−0.25	−0.52	−0.22	−0.70	−0.06	−0.03	0.09	0.09	0.28	0.25	0.27	0.19	0.28	0.29
10	−0.65	−0.28	0.29	−0.22	0.29	0.68	0.90	0.89	0.71	1.00	−0.18	−0.74	−0.39	−0.76	0.19	−0.55	−0.64	−0.63	0.03	0.04	0.44	0.30	0.54	0.36	0.54	0.35
11	0.75	−0.10	0.30	−0.11	−0.07	0.35	−0.39	−0.25	−0.27	−0.18	1.00	0.43	0.94	0.39	0.83	0.49	0.03	0.06	−0.08	−0.05	0.05	0.06	−0.24	−0.15	−0.23	−0.30
12	0.79	0.16	−0.09	0.09	−0.16	−0.59	−0.77	−0.70	−0.59	−0.74	0.43	1.00	0.60	0.99	0.04	0.84	0.63	0.60	0.03	−0.05	−0.37	−0.25	−0.65	−0.41	−0.61	−0.42
13	0.79	−0.08	0.22	−0.06	−0.18	0.12	−0.51	−0.33	−0.25	−0.39	0.94	0.60	1.00	0.60	0.59	0.50	0.34	0.37	−0.08	−0.05	−0.08	−0.01	−0.42	−0.27	−0.39	−0.36
14	0.74	0.16	−0.11	0.10	−0.20	−0.60	−0.74	−0.66	−0.52	−0.76	0.39	0.99	0.60	1.00	−0.06	0.74	0.73	0.71	0.03	−0.05	−0.38	−0.24	−0.66	−0.42	−0.61	−0.42
15	0.50	−0.10	0.33	−0.15	0.11	0.63	−0.10	−0.06	−0.22	0.19	0.83	0.04	0.59	−0.06	1.00	0.35	−0.47	−0.44	−0.07	−0.03	0.24	0.16	0.10	0.08	0.08	−0.13
16	0.79	0.15	−0.01	0.04	0.00	−0.43	−0.73	−0.69	−0.70	−0.55	0.49	0.84	0.50	0.74	0.35	1.00	0.15	0.11	0.04	−0.04	−0.27	−0.19	−0.48	−0.26	−0.50	−0.37
17	0.27	0.07	−0.19	0.12	−0.28	−0.58	−0.45	−0.32	−0.06	−0.64	0.03	0.63	0.34	0.73	−0.47	0.15	1.00	0.98	0.03	−0.03	−0.37	−0.22	−0.57	−0.40	−0.49	−0.26
18	0.27	0.07	−0.19	0.14	−0.26	−0.53	−0.43	−0.30	−0.03	−0.63	0.06	0.60	0.37	0.71	−0.44	0.11	0.98	1.00	0.05	0.00	−0.31	−0.16	−0.53	−0.37	−0.48	−0.26
19	−0.09	0.08	0.06	0.04	0.00	−0.14	−0.03	0.07	0.09	0.03	−0.08	0.03	−0.08	0.03	−0.07	0.04	0.03	0.05	1.00	0.80	0.33	0.30	0.28	0.30	0.21	0.10
20	−0.09	0.02	0.03	0.06	−0.03	−0.02	0.02	0.08	0.09	0.04	−0.05	−0.05	−0.05	−0.05	−0.03	−0.04	−0.03	0.00	0.80	1.00	0.27	0.29	0.24	0.21	0.10	0.00
21	−0.23	−0.19	0.21	−0.06	0.05	0.45	0.37	0.38	0.28	0.44	0.05	−0.37	−0.08	−0.38	0.24	−0.27	−0.37	−0.31	0.33	0.27	1.00	0.90	0.51	0.38	0.43	0.10
22	−0.16	−0.17	0.10	0.04	0.02	0.30	0.25	0.29	0.25	0.30	0.06	−0.25	−0.01	−0.24	0.16	−0.19	−0.22	−0.16	0.30	0.29	0.90	1.00	0.33	0.32	0.20	0.02
23	−0.46	−0.01	0.15	−0.05	0.11	0.49	0.53	0.41	0.27	0.54	−0.24	−0.65	−0.42	−0.66	0.10	−0.48	−0.57	−0.53	0.28	0.24	0.51	0.33	1.00	0.76	0.78	0.53
24	−0.30	−0.02	0.06	0.06	0.15	0.31	0.34	0.28	0.19	0.36	−0.15	−0.41	−0.27	−0.42	0.08	−0.26	−0.40	−0.37	0.30	0.21	0.38	0.32	0.76	1.00	0.52	0.55
25	−0.45	−0.08	0.23	−0.19	0.05	0.47	0.53	0.42	0.28	0.54	−0.23	−0.61	−0.39	−0.61	0.08	−0.50	−0.49	−0.48	0.21	0.10	0.43	0.20	0.78	0.52	1.00	0.49
26	−0.40	−0.04	0.01	0.02	0.10	0.20	0.40	0.34	0.29	0.35	−0.30	−0.42	−0.36	−0.42	−0.13	−0.37	−0.26	−0.26	0.10	0.00	0.10	0.02	0.53	0.55	0.49	1.00

Three parameters were chosen as the basis of clustering. The remaining ones were used to quantify other features of the cells, once the clusters had been created.
1) XY dendritic field area, as measured by tightest fitting convex polygon around z-collapsed cell.
2) Mean stratification depth of dendritic arbor in IPL, measured as % depth from the inner nuclear layer to the ganglion cell layer
3) Standard deviation of dendritic arbor stratification depth in the IPL, measured as a % of the depth from the INL to the GCL.
4) Distance in microns from cell body to mean dendritic arbor stratification along z-axis.
5) Asymmetry value; distance between cell body and dendritic arbor centers of mass/dendritic arbor average radius.
6) Number of branch points within dendritic arbor.
7) Number of branch points/XY dendritic field area.
8) Total dendritic length/XY dendritic field area.
9) Total terminal dendritic segment length (see 13)/XY dendritic field area.
10) Total nodal dendritic segment length (see 15)/XY dendritic field area.
11) Total dendritic length.
12) Mean dendritic segment length.
13) Total terminal dendritic segment length; terminal segments begin at a branch point and terminate without branching.
14) Mean terminal dendritic segment length; terminal segments begin at a branch point and terminate without branching.
15) Total nodal dendritic segment length; nodal segments begin at a branch point and end at another branch point.
16) Mean nodal dendritic segment length; nodal segments begin at a branch point and end at another branch point.
17) Total terminal dendritic segment length/total nodal dendritic segment length.
18) Mean terminal dendritic segment length/mean nodal dendritic segment length.
19) Segment tortuosity mean–actual dendritic length from branch point to next branch point or end/straight line distance.
20) Segment tortuosity standard deviation–actual dendritic length from branch point to next branch point or end/straight line distance.
21) Nodal tortuosity mean–actual dendritic length from start of proximal dendrite to any branch point/straight line distance.
22) Nodal tortuosity standard deviation–actual dendritic length from start of proximal dendrite to any branch point/straight line distance.
23) Planar angle mean–3D angle at branch point between straight lines extending directly to successive branch points.
24) Planar angle standard deviation–3D angle at branch point between straight lines extending directly to successive branch points.
25) Local spline angle mean–3D angle formed at branch point between nearest recorded points of daughter branches.
26) Local spline angle standard deviation–3D angle formed at branch point between nearest recorded points of daughter branches.

(Sinha, 2002). As for face recognition, the availability of computing power and imaging technology raises the possibility that the informal criteria traditionally used can be replaced by a more rigorous method of classification. One of our goals here was to explore such a classification.

We studied the mouse retina because of its many advantages for genetic manipulation. We used a variety of cell-filling methods, which now can quite readily generate large samples of well-stained neurons (Tauchi and Masland, 1984; Gan et al., 2000; Feng et al., 2000; Dacey et al., 2003). Every neuron was imaged in three dimensions by digital microscopy. The ganglion cells of the mouse turn out to be a particular challenge, as they are much less distinctive, one from the other, than are the ganglion cells of the monkey, cat, or rabbit (Roska and Werblin, 2001; O'Brien et al., 2002; Rockhill et al., 2002; Dacey et al., 2003). However, from our measurements we gain much useful information, and a preliminary classification will be presented and compared with earlier ones (Doi et al., 1995; Sun et al., 2002; Badea and Nathans, 2004). We also learned some of the limitations of this methodology and these will be described.

MATERIALS AND METHODS

Individual ganglion cells were labeled in C57/Bl6 with either DiI or DiO using standard biolistic technique (Gan et al., 2000) or Lucifer yellow injections (Rockhill et al., 2002). Labeled ganglion cells were also observed in GFP-M transgenic mice, generously donated by Dr. J. Sanes. In these mice a small number of retinal ganglion cells strongly express GFP (Feng et al., 2000).

All mice were anesthetized with ketamine (30–40 mg/kg) and xylazine (3–6 mg/kg) in accordance with institutional guidelines. The animals were then euthanized by an overdose of the same agents. All procedures were in accord with protocol number 2002N0003 3/2 of the animal care committee of the Massachusetts General Hospital.

Both eyes were removed and immersed in carboxygenated Ames' Medium (A1420, Sigma, St. Louis, MO). The retinas were teased free of the vitreous and sclera and an orienting mark and four curvature relieving cuts were made in the retina. The retinas from transgenic mice and the retinas for intracellular injections were counterstained immediately with 4′,6-Diamidino-2-phenylindole

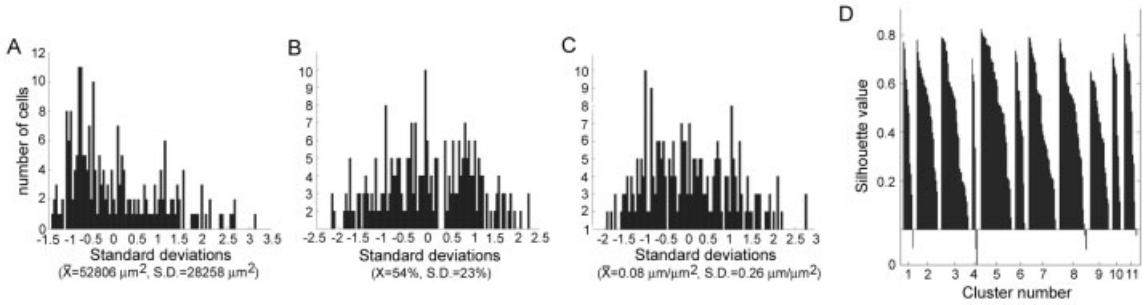

Fig. 1. Distributions of values for each of the three major parameters: **A:** Dendritic XY coverage area. **B:** Mean dendritic stratification depth. **C:** Average dendritic density (length of dendrite per unit area). For each parameter all values have been rescaled to the number of standard deviations from the mean. **D:** Silhouette values for the 11-cluster solution. The silhouette plot shows the individual silhouette values for the entire cell population grouped by cluster and ordered from highest to lowest within each cluster. The silhouette value of a cell compares that cell's distance to cells in its own cluster against that cell's distance to cells in the closest cluster.

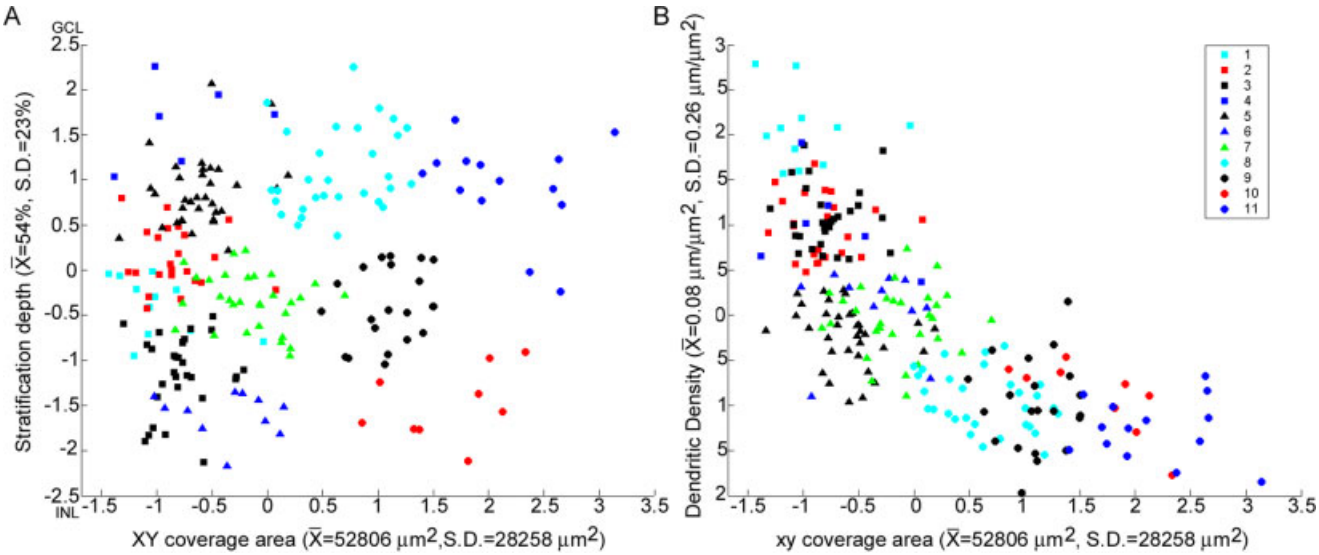

Fig. 2. **A:** Coverage area plotted against mean cell depth for the entire cell population, depicted as groups by cluster. **B:** Coverage area plotted against dendritic density.

(DAPI) (D-0542, Sigma). For Lucifer yellow injections 160 µl of a 1% stock solution of DAPI was diluted in 10 ml of carboxygenated Ames' Medium and for GFP-M labeled-retinas 300 µl of a 1% stock solution of DAPI was diluted in 10 ml of carboxygenated Ames' Medium. All incubations were done in the dark on a rocker at room temperature. Retinas for Lucifer yellow injections were incubated for 10 minutes and GFP-M-labeled retinas were incubated for 1 hour. Following DAPI labeling all retinas were washed 3 × 10 minutes in carboxygenated Ames' Medium. GFP-M retinas were fixed in 4% paraformaldehyde (18505, Ted Pella, Redding, CA) for 1 hour and then washed in 0.1 M phosphate buffer (pH 7.4) (3 × 10 minutes). Following fixation all retinas were mounted in Vectashield (H1000, Vector Laboratories, Burlingame, CA) and observed immediately.

The biolistics technique has been described by Gan et al. (2001) and Wang et al. (1996). Briefly, 100 µl of methylene chloride was added to 30 mg of 0.4 µg tungsten beads (1652265, Bio-Rad Laboratories). The mixture was sonicated and then poured onto a glass slide. After the beads had dried onto the slide, 3 mg of 1,1′-dioctadecyl-3,3,3′,3′-tetramethylindocarbocyanine perchlorate (DiI) (D282, Molecular Probes, Eugene, OR) or 3,3′-dioctadecyloxacarbocyanine perchlorate (DiO) (D275, Molecular Probes) or a mixture of DiI and DiO dissolved in 100 µl of methylene chloride was evenly applied to the beads. The DiI- or DiO-coated tungsten beads were then scraped off the slide and placed in 3 ml of distilled water. The beads were sonicated for 5 minutes. The tubing prep station (165-2418, Bio-Rad) was used to coat the inside of the tubing with the DiI- or DiO-coated tungsten beads. The coated tubing was loaded into the Helios Gene Gun (165-2431, Bio-Rad) and the retinas were shot, ganglion cell side up, at 60–70 psi. The retinas were then rocked in 5.8×10^{-5}M DAPI in carboxygenated Ames' Medium at room temperature for 20 minutes and washed 3 × 10 minutes in carboxygenated Ames' Medium, fixed, and mounted as previously described.

Intracellular injections were performed following the methods previously described (Tauchi and Masland, 1985;

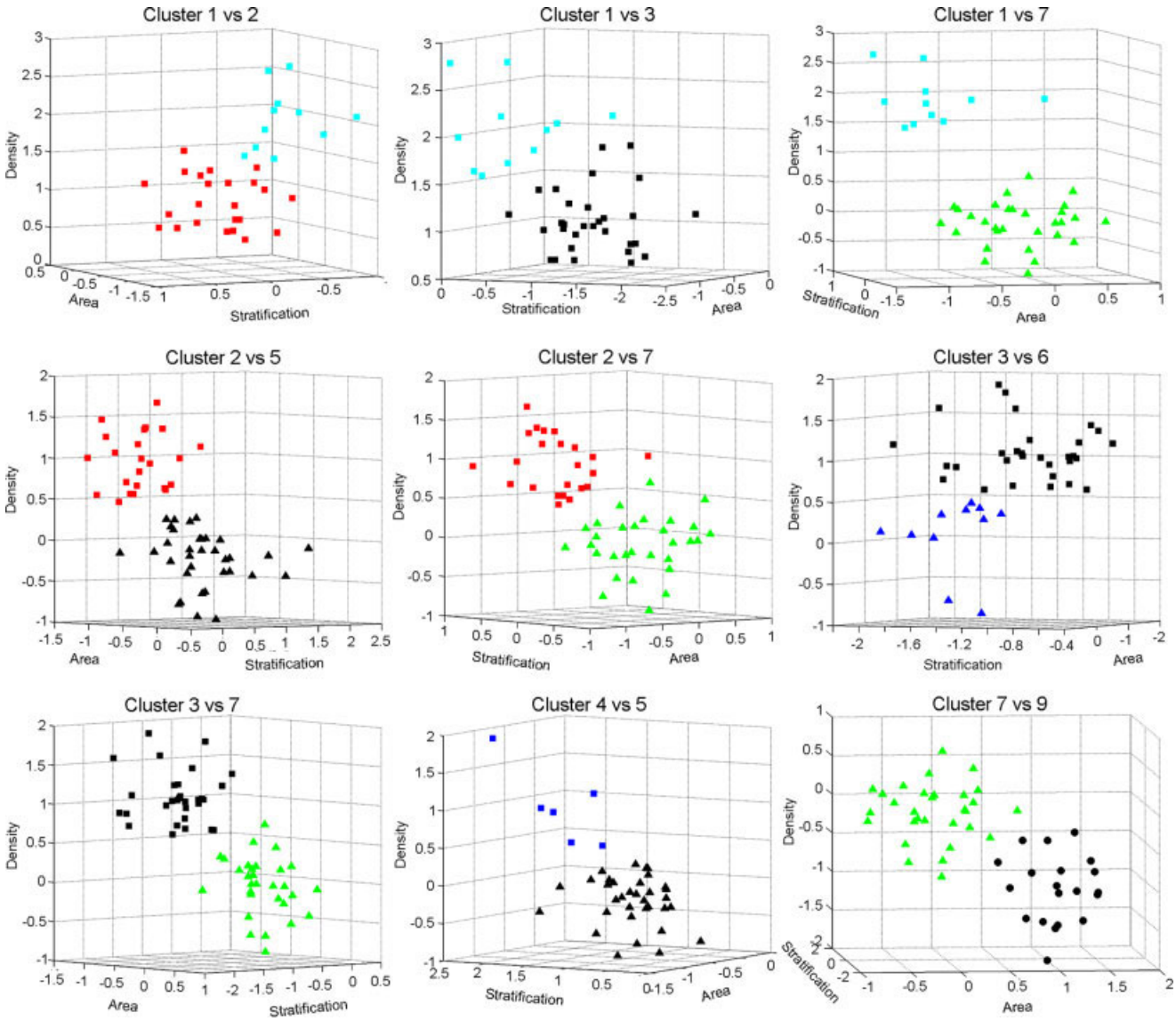

Fig. 3. Pairwise 3D visualizations of cluster spatial separation for pairs difficult to separate in two dimensions alone. The existence of these separations verifies the individual identities of these groups. Note that 2D clustering satisfactorily resolves some, but not all of the clusters.

Lin et al., 2004). The retinas were labeled with DAPI as previously described and then placed on Millipore filter paper (AABPO4700, Millipore, Billerica, MA). The retinas were then placed in a superfusion chamber on a fixed stage Leitz microscope. Using a 40× water immersion objective (Achroplan, NA 0.75, Zeiss) DAPI-labeled ganglion cells were injected with 4% Lucifer yellow (L0144, Sigma) in 0.1 M phosphate buffer, pH 7.6. Retinas were then fixed and mounted as previously described and immediately observed.

All retinas were observed by epifluorescence on a Zeiss Axioplan equipped with a Princeton Instruments MicroMax cooled CCD camera. Z-stacks (1-μm steps) were taken using Metamorph (v. 3.0, Universal Imaging, Downingtown, PA) to drive a focus motor (Ludl Electronic Products, Hawthorne, NY). Corresponding z-stacks were taken for GFP, DiI, DiO, or Lucifer yellow-labeled cells and DAPI. The morphology of the cells was shown by the GFP, DiI, DiO, or Lucifer yellow; their stratification was determined relative to the DAPI-labeled nuclei of the inner nuclear layer or ganglion cell layer (MacNeil and Masland, 1998; MacNeil et al., 1999).

All of the cells included in this study came from the central three-quarters of the retinal surface. The gradient of density for ganglion cells (and other retinal neurons) in the mouse is much less steep than in the rabbit, cat, or monkey (Jeon et al., 1998) and the slight variation in ganglion cell size seemed to outweigh the loss of the cells that would be discarded were location more tightly controlled. (It would be interesting to know if there are distinct types of ganglion cells associated with the region of retina to which short wavelength cones are restricted, but

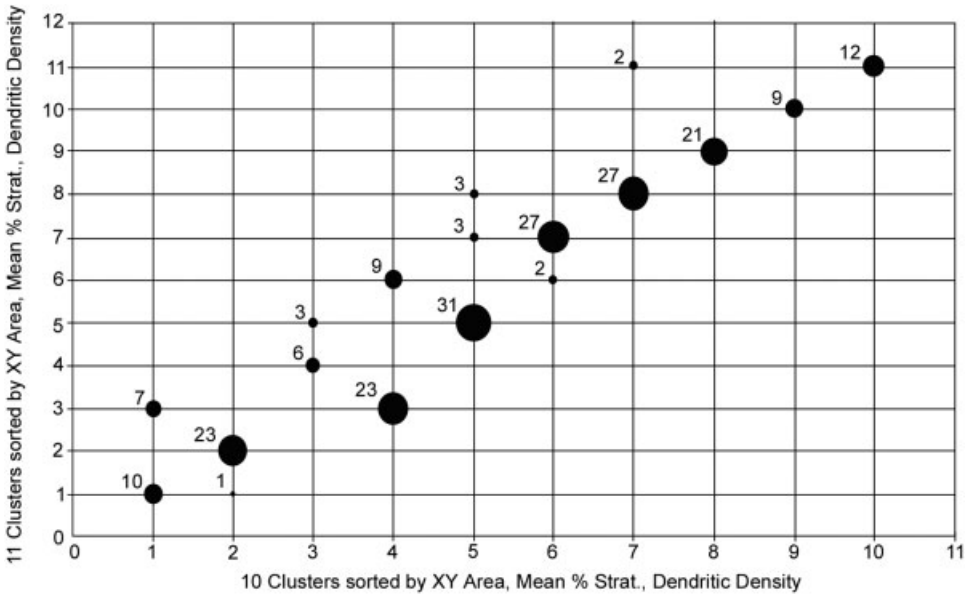

Fig. 4. The stability of the clusters. Here the algorithm was forced to create 10 clusters or 11 clusters. The size of the symbols shows how many cells were contained in a cluster. Constraining the number of clusters caused "movement" of a few of the cells, but the fundamental clustering is little changed; the basic identification of cells as belonging to a group remained the same.

we did not track location precisely enough to answer the question.)

The contrast and brightness of the micrographs shown here were adjusted using Adobe PhotoShop (San Jose, CA).

Digital representations

Cells were manually traced using the Neurolucida analysis software (Neurolucida v. 4.36, Microbrightfield, Williston, VT). To maintain an unbiased cell population, we traced all available cell stacks, so long as the images were robust enough that an accurate depiction of the dendritic morphology could be obtained. Metamorph stacks were converted to TIF files, opened in Neurolucida, and a reference point was established at the z-plane where the cell body was in focus. The cell body was outlined and then the dendrites and axon were traced by toggling up and down through the cell stack while tracing the dendrites and axon. The end result was a 3D "stick-figure" of the cell.

Some imaged cells were unusable because of incomplete filling, excessive overlaps among cells, lack of a detectable axon, or tissue deformation. In total, 219 3D cell tracings were used for analysis. Images of GFP-expressing cells proved to be clearer and more accurate than other staining methods, as their cell bodies and processes were fully intact and filled with dye to the utmost dendritic tips. Thus, GFP-expressing cells comprised 191 of the tracings analyzed. Images of cells microinjected with Lucifer yellow dye were more prone to be underfilled, and often dye leaked from the cell body, obscuring the cell's proximal dendrites; 19 tracings of Lucifer yellow-injected cells were used in analysis. DiOlistically labeled cells, while less likely to have underfilled dendrites than Lucifer yellow microinjected cells, characteristically had bright flare around the cell body, obscuring the cell's proximal dendritic arbors; only nine tracings of DiOlistically labeled cells were used in the final analysis.

Selecting and measuring morphological parameters

We calculated some 42 parameters (see Supplementary Data). Some of them were found to be uninformative, usually because they were redundant in one way or the other. Twenty-six of the most useful are shown in Table 1.

When classifying cells, selection of an appropriate parameter space is an influential decision. Cells are grouped by their distribution of morphologic parameters; each additional parameter adds a new dimension by which cells can be separated, but decreases all other individual parameters' importance in distinguishing between cell types. A correlation matrix is shown in Table 1. It is notable that there are high correlations among many of the parameters. Sometimes these are obvious: the length between nodes (parameter 16) is negatively correlated with the number of nodes (parameter 7) because a cell with many branch points has a shorter average distance between the branch points than a sparsely branched cell. Sometimes they are less so, as is the high correlation between branch angle (parameter 23) and density of branch points (parameter 7). The selection of parameters thus becomes a complex, and ultimately somewhat empirical issue. Weighting of parameters was avoided to reduce human bias in the classification. After substantial preliminary work (Fish, 2003) a set of three parameters was chosen as the basis of clustering. They were chosen in part empirically, from experiments in which various parameter sets were evaluated by silhouette analysis, and in part from the principle that cellular features of known physiological significance were most likely to be effective ways to discriminate among the cells. A set of only three parameters was chosen in order to minimize the experimental noise that accumulates with each added measurement (see Discussion).

The first parameter is the retinal coverage area of the ganglion cell (Fig. 1A). The size of a ganglion cell's receptive field determines the size of the visual space upon which that ganglion cell reports. This parameter is mea-

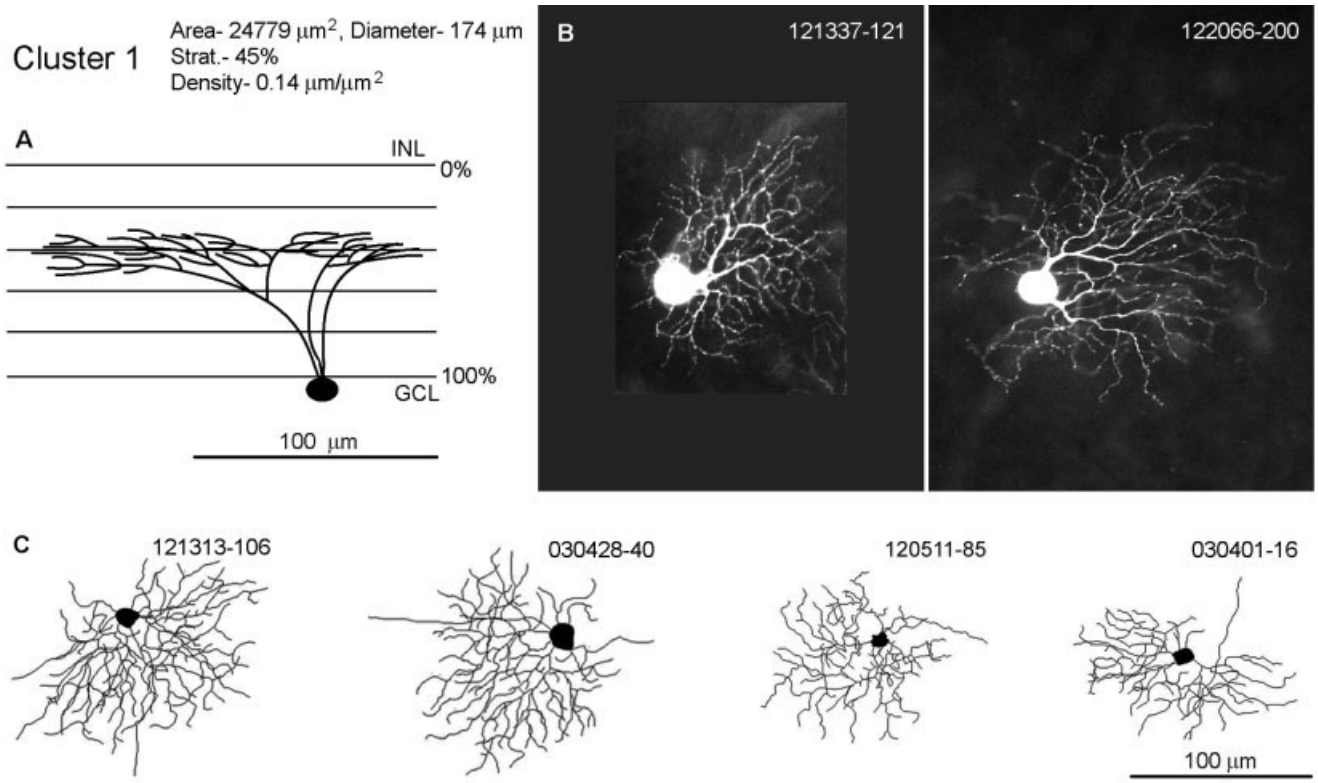

Fig. 5. Cells included in cluster 1. In this figure and Figures 6–15 cells from each of the clusters identified by the k-means classification are shown. The name of the cluster and its three defining parameters—dendritic field spread, level of stratification, and spatial density of dendrites within the field—are indicated in **A**. The "diameter" expressed is the calculated mean diameter assuming a circular dendritic field of the same area as the area measured for the cells. Micrographs of one or more cells are shown in **B**. **C:** Line drawings of the dendritic structure; these are the computerized representations on which the clustering was carried out. Scale bars = 100 μm.

sured as the area of the smallest 2D convex polygon possible around a projection of the cell's dendritic arbor when collapsed along the z-axis. The second parameter is the mean stratification depth of the ganglion cell's dendritic arbor within the inner plexiform layer (Fig. 1B). The depth of bipolar and amacrine axon terminals in the inner-plexiform layer varies by type (MacNeil and Masland, 1998; Ghosh et al., 2004; Pignatelli and Strettoi, 2004; Badea and Nathans, 2004), so the depth at which a ganglion cell's dendritic arbor lies determines the types of axons that synapse on the cell.

This parameter is measured using data from the corresponding DAPI stack to define the limits of the IPL. To calculate the stratification distribution, we employed a broadly useful analysis tool in the Neurolucida package—a 3D, cylindrical binning operation known as 3D Wedge analysis. (This function was also used for many of the other measurements shown in Table 1.) To calculate stratification, we binned dendritic arbors into stacked 1-μ-thick discs, making a discrete (noncontinuous) stratification distribution. This distribution was then mapped onto the inner plexiform layer, using the z-stack of the same region viewed by DAPI staining as a way to visualize the margins of the inner plexiform layer. The depth of stratification of a particular cell was directly measured as the mean depth of the dendrites within the layer.

The third parameter is the density of processes of the dendritic arbor (Fig. 1C). The density of dendritic processes is indicative of the number of bipolar and amacrine axonal inputs the cell receives within its given area of influence. This parameter is measured as the total length of the dendrites divided by the coverage area of the dendritic arbor.

Because these three parameters differ in both their units and in their ranges of values, each parameter was individually normalized for the whole cell population to a mean of zero and a standard deviation (SD) of one. With this normalization, the distance between any two points in the parameter space is simply the distance between them in a Cartesian 3D space, given as the Euclidean distance between the points, $d_{ij}^2 = (\mathbf{x}_i - \mathbf{x}_j)(\mathbf{x}_i - \mathbf{x}_j)'$.

Grouping cells by parameters

Cells (or any items that can be represented by parametric measurements of properties of interest) can be grouped by the variance in their parameters. We experimented with diverse methods for clustering cells (Fish, 2003), but settled on the k-means partitioning technique (Kaufman and Rousseeuw, 1990). This method optimizes the set of clusters with respect to the distance between each point and the centroid of its cluster, summed for all points. The algorithm proceeds as follows. A set of k random points to be used as initial cluster centroids is generated. Each point is assigned to the cluster with the closest centroid. The cluster centroids are then recalculated based on the points assigned to each cluster. The points are then reas-

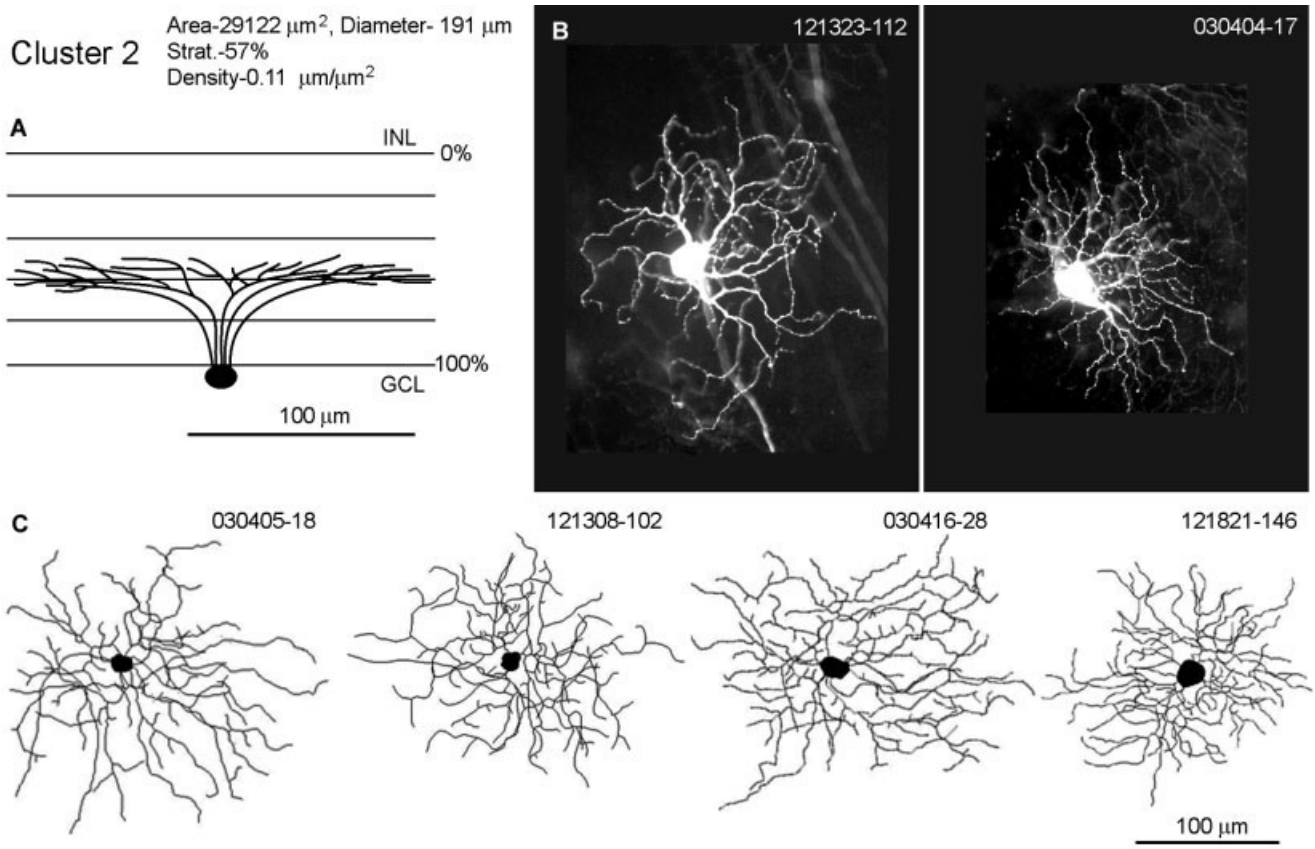

Fig. 6. Cells included in cluster 2. Conventions as in Figure 5.

signed to clusters based on their proximity to the new centroids, and then the centroids are again recalculated. This process continues until all points cease changing their cluster designations. Finally, each point is individually tested to see if changing its cluster designation will decrease the sum of all point-to-own-cluster-centroid distances. Any time moving a point decreases this sum, centroids are recalculated and the testing of points begins anew.

Two main issues exist regarding the use of this method. Like most optimization methods, k-means is a hill-climbing algorithm, where an arbitrary starting point is iteratively improved until it cannot be improved further. Therefore, the algorithm will always find the best solution for a given starting point, but might not find the best overall solution. To avoid this problem, we performed the k-means partitioning on the dataset 10,000 times and took the best answer. This was then repeated twice more (for a total of 30,000 repetitions) and the final answer was only accepted as best if reached all three times.

The second issue is that an initial number of clusters k must be supplied. This is more problematic, as the correct value for k is unknown. To address this problem, we performed the k-means analysis for every number of clusters from 3 to 20. This range was chosen by mandating that, for n cells in our dataset, the n/k ratio, or the average number of cells per group, must fall within the range of 10 to 100. The upper limit of $n/k \leq 100$ ensures that we will find at least three different cell types, which is widely expected due to recordings taken from the ganglion cells. The lower limit of $n/k \geq 10$ discards solutions with large numbers of clusters, as classification systems with less than 5% of the total population in each class on average tend to produce several classes so small that they comprise 1% or less of the total population. Although low-density cell types certainly exist, they can only achieve a complete retinal coverage when their dendritic arbors are very broad (Wässle et al., 1981; Rockhill et al., 2000).

We then had to choose the best overall clustering from the best clustering for each possible number of clusters. To choose between clusterings with different numbers of groups, our strategy was to optimize the average silhouette value for all points, as described by Kaufman and Rousseeuw (1990) The silhouette value, s, for a single point i in cluster c is defined as:

$$s(i) = (b(i)–a(i))/\text{maximum}(a(i),b(i))$$

where a(i) is the average distance from point i to all other points in cluster c and b(i) is the average distance between i and all other points in the cluster for which b(i) is smallest, excluding cluster c. This is a ratio of the closeness of a point to the other points in its own cluster versus the points in the nearest cluster, and approaches theoretical limits of 1 for a perfectly clustered point, 0 for a completely ambiguously clustered point, and –1 for a completely inappropriately clustered point (Fig. 1D).

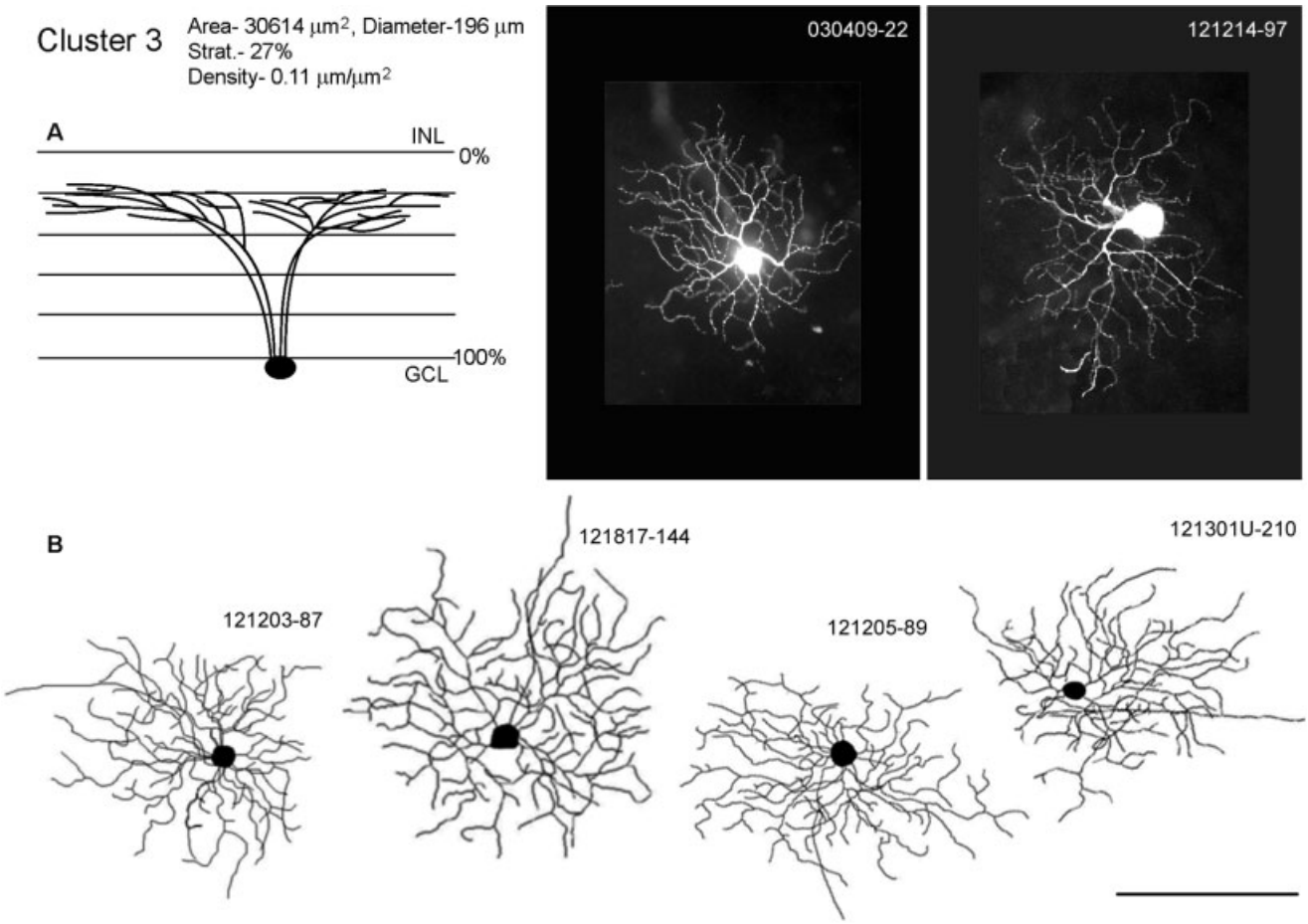

Fig. 7. Cells included in cluster 3. Conventions as in Figure 5.

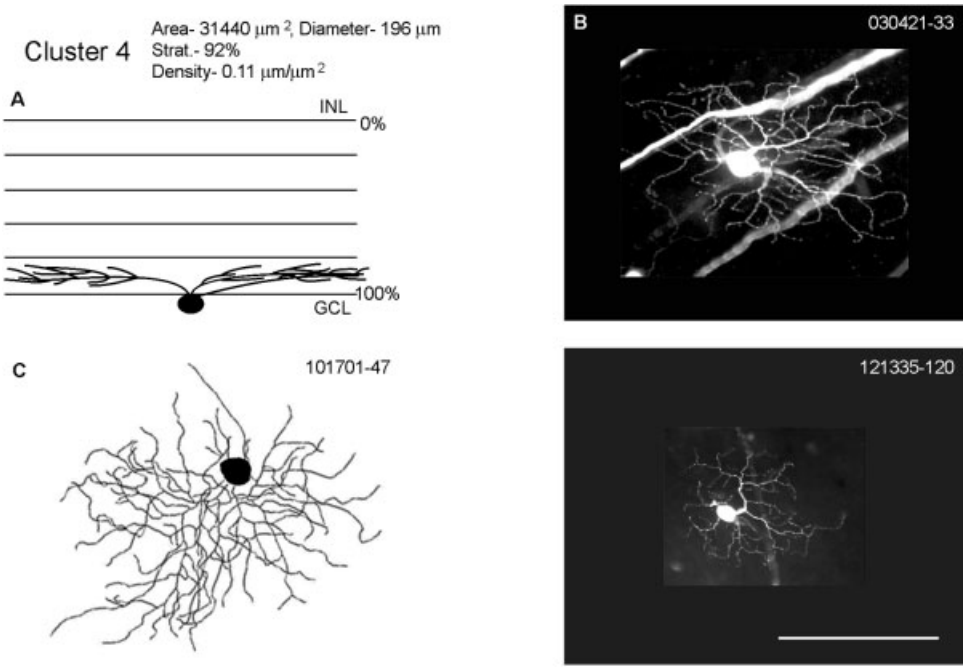

Fig. 8. Cells included in cluster 4. Conventions as in Figure 5.

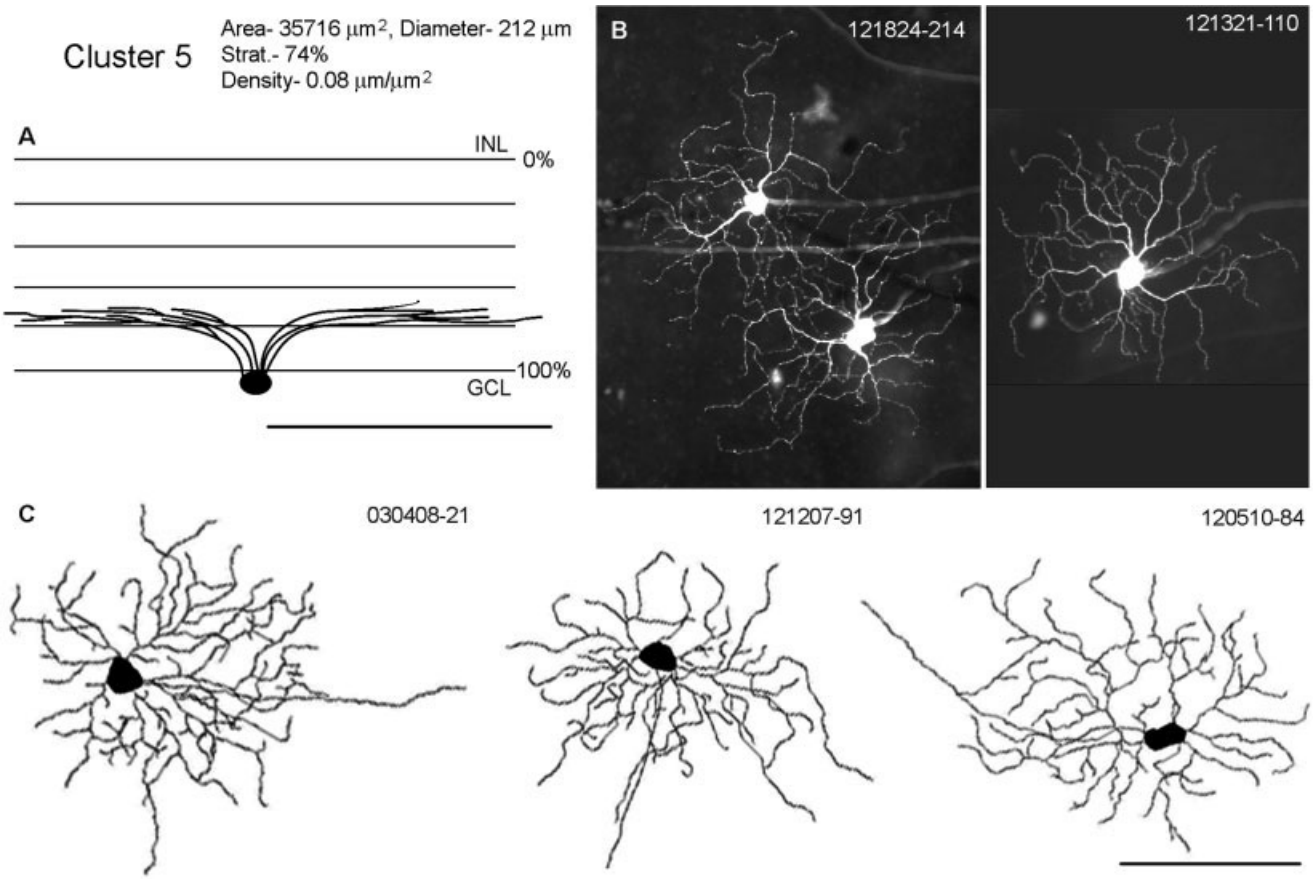

Fig. 9. Cells included in cluster 5. Conventions as in Figure 5.

RESULTS

By optimizing the average silhouette value for all points, we found our best k-means solution for 11 groups to be the best overall solution. The silhouette value is a ratio comparing the average parametric similarity of a cell to the members of its own cluster versus that cell's average similarity to the cells in the nearest cluster. A plot of the silhouette values for all cells, arranged into the 11 clusters, is given in Figure 1D, and qualitatively demonstrates the cohesiveness of each cluster. This plot suggests that group four is the least cohesive, as it has few archetypal cells with high silhouette values located at the center and more than one cell with a negative silhouette value, which signifies better correspondence to another group. Group five, alternatively, appears most cohesive with many cells with high silhouette values densely crowded at the core of the cluster and the remainder spanning out with slowly and evenly decreasing silhouette values.

The clusters are illustrated in 2D views in Figure 2. Here the parametric groupings of the cell classes are spatially apparent. To resolve ambiguity between pairs of cells whose separation appears uncertain in the 2D view, a subset of clusters are shown in three dimensions in Figure 3. These were chosen to resolve the most ambiguous of the pairs; the others are readily separated using only two dimensions, as shown in Figure 2.

To verify the consistency of this solution, we compared it to the best k-means solutions for 10, 12, and 13 clusters. If a relationship between two cells is defined as being whether they are in the same class or in two different classes, then changing the number of clusters does not significantly change the total relationships between cells. We measured this by computing the number of times that a pair of cells moved from sharing a cluster to occupying two different clusters. Only 4.34%, 2.14%, and 2.17% of relationships between all possible pairs of cells changed when 11 clusters were compared against the best clusterings for 10, 12, and 13 classes, respectively. The insignificance of these changes is further emphasized by the fact that changing the number of clusters inflexibly requires that some changes in assignment of cells to clusters are forced to occur. The relationship between 10 and 11 cluster classifications is shown in Figure 4.

Cluster descriptions

The cells were clustered solely on the basis of three parameters: dendritic field area, mean dendritic stratification depth, and dendritic length per unit field area. The clusters formed by these parameters alone often appeared to contain cells similar along other dimensions, not used in our basic clustering process (Table 1), frequently those traditionally used to describe the morphological character

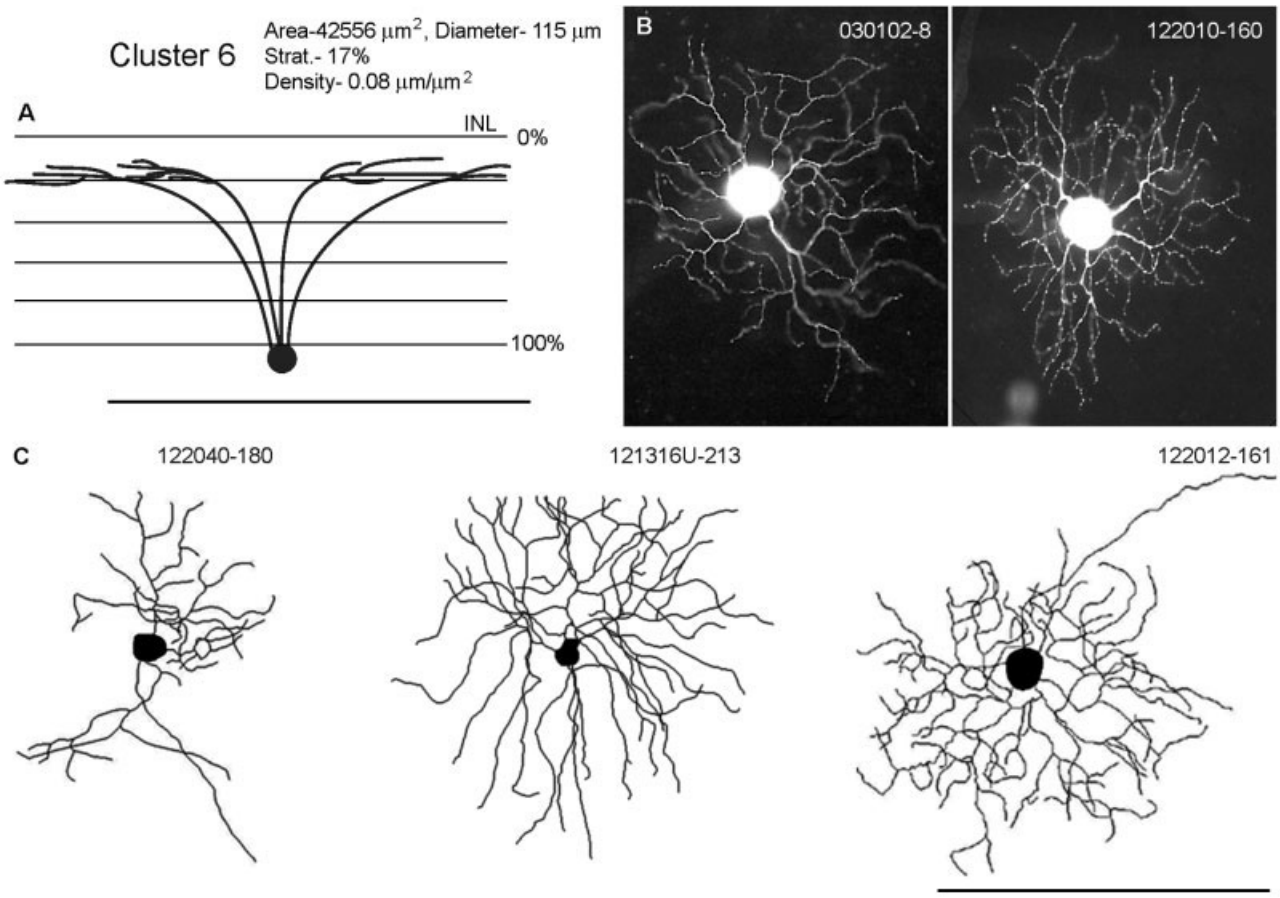

Fig. 10. Cells included in cluster 6. Conventions as in Figure 5.

of dendritic arbors. Below, we will comment on those other aspects and compare the cells to those identified in earlier surveys. For each cluster the values within that cluster of 42 measured or derived morphological parameters are available as Supplementary Data on this journal's website (see first-page footnote). For comparability, the values of parameters other than the three main ones (depth, area, process density) are expressed as the number of SDs above or below the mean for the whole population of cells. For example, a value of +1.3 would mean that the cells within that cluster had values for that parameter that averaged 1.3 SDs above the mean for all cells.

Cluster 1 is the smallest and densest group of cells (Fig. 5). They stratify at 45% of the IPL, with a density of 0.14 $\mu m/\mu m^2$ and a dendritic field diameter of 174 μm. Cluster 1 cells typically have 5–6 primary dendrites and the proximal portion of 1–2 of those primary dendrites are thick and taper quickly. These are the most broadly stratified of all the cells, 0.89 SD above the population mean on our measure of stratification thickness. Other characteristics typical of this cluster are that the dendrites often end in hooks. The cells are slightly asymmetric. Cluster 1 cells appear similar to Sun et al.'s (2002) RG_{B2} cells which stratify at 33 ± 16%, have a field diameter of 135 ± 37 μm, and have a dense dendritic field; and to cluster 1 of Badea and Nathans (2004).

Cluster 2 cells, similar to Badea and Nathans' cluster 2, stratify at 57% of the IPL, have a density of 0.11 $\mu m/\mu m^2$, and a dendritic field diameter of 191 μm (Fig. 6). These cells have 4–6 primary dendrites. The dendrites of cluster 2 make large, sweeping turns and branch at broad angles. The mean branch angle was 0.94 SD above the population mean. Short terminal branches often come off perpendicular to the main branch. These branches were short: the mean length of terminal dendrites was 0.86 SD below the population mean. Cluster 2 cells look very similar to Sun et al.'s (2002) RG_{B1} cells, which stratify at 38 ± 16% and have a dendritic field diameter of 223 ± 41 μm.

Cluster 3 cells stratify at 27%, have a density of 0.11$\mu m/\mu m^2$ and a dendritic field diameter of 196 μm (Fig. 7). Cluster 3 cells have 4–7 primary dendrites and look very similar to cluster 2 cells, but the dendrites do not branch as broadly (mean branch angle +0.05 SD). This is reflected in many, short perpendicular secondary and tertiary branches. Cluster 3 cells resemble to Sun et al.'s (2002) RG_{C5} cells and Badea and Nathans' (2004) cluster 3. RG_{C5} cells stratify at 39 ± 12% and have a dendritic field diameter of 212 ± 37 μm.

Cluster 4 cells stratify at 92%, have a density of 0.11 $\mu m/\mu m^2$, and a dendritic field diameter of 196 μm (Fig. 8). The cells in cluster 4 have 4–6 primary dendrites. The dendrites are straighter than dendrites of

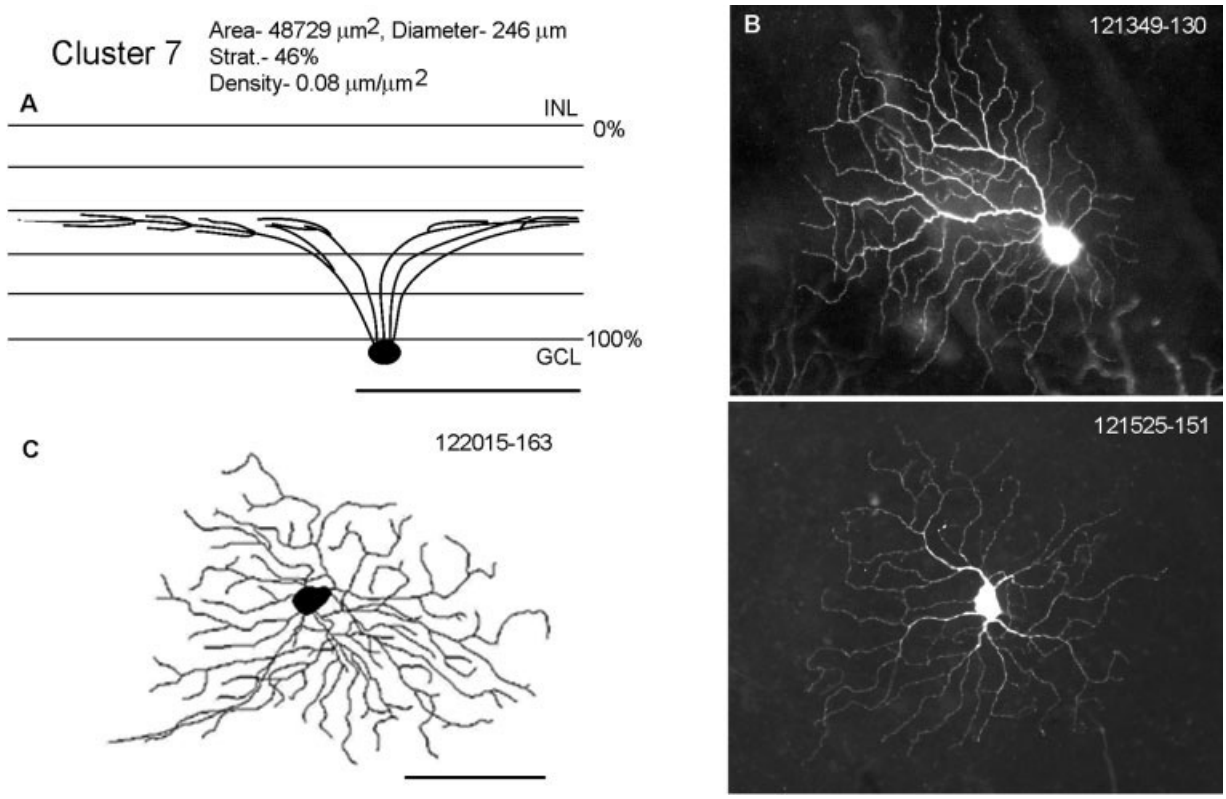

Fig. 11. Cells included in cluster 7. Conventions as in Figure 5.

the cells in clusters 2 and 3: the mean tortuosity was positive for clusters 1–3 and −0.39 SD for cluster 4. Cluster 4 cells look somewhat similar to Sun et al.'s (2002) RG_{B3} (outer) cells, which stratify at 67 ± 10% and have a dendritic field diameter of 199 ± 47 μm. There was no similarly small cell that stratified low in the IPL in the clustering of Badea and Nathans (2004).

Cluster 5 cells stratify at 74%, with a density of 0.08 $\mu m/\mu m^2$—noticeably less dense than the cells in clusters 1–4. They have a dendritic field diameter of 212 μm (Fig. 9). The cells in this group have 5–7 primary dendrites. We nicknamed this group the "octopus" cells because the wavy dendrites radiating from the cell body looked like the tentacles on an octopus. Cluster 5 had the lowest variance on the main parameters of any of our groups and was thus the most cohesive. Cluster 5 cells look similar to Sun et al.'s (2003) RG_{C2} (outer) cells, which stratify at 75 ± 7% and have a dendritic field diameter of 283 ± 63 μm. They resemble cluster 5 of Badea and Nathans (2004).

Cluster 6 was an amorphous group. The k-means algorithm defined them as a cluster, distinct from the other cells, because they are relatively homogeneous in size (115 μm in diameter), density (0.08) $\mu m/\mu m^2$, and mean level of stratification (17% of the IPL). Within those bounds, however, there was much heterogeneity in the detailed dendritic morphology and we strongly suspect that this cluster includes cells that would traditionally be classified as more than a single cell type. Five of our total sample of 26 cells are shown in Figure 10. Four of these look quite similar, but the fifth, though meeting the numerical criteria of this cluster, has a less dense and less symmetric dendritic arbor. These cells are so different in morphological detail that their status as an independent functional group is doubtful. Badea and Nathans' (2004) cluster 6 will be discussed below.

Cluster 7 cells stratify at 46%, have a density of 0.08, and a dendritic field diameter of 246 μm (Fig. 11). This group has 5–8 primary dendrites. The dendrites in this group radiate out and branch at regular intervals, giving the arbor a somewhat ladder-like appearance. The dendrites are not as wavy as the dendrites of cells in clusters 1–5, with an average tortuosity near the population mean (−0.01 SD). Cluster 7 cells look very similar to Sun et al.'s RG_{A2} (inner) cells, which stratify at 38 ± 12% and have a dendritic field diameter of 282 ± 65 μm.

Cluster 8 cells stratify at 80%; have a density of 0.06 $\mu m/\mu m^2$ and a dendritic field diameter of 300 μm (Fig. 12). These cells have 4–6 primary dendrites that radiate out, branch at fairly narrow angles (−0.39 SD), and rarely overlap. The dendrites in this group are also fairly straight. Cluster 8 cells look similar to Sun et al.'s RG_{A2} (outer) cells, which stratify at 71 ± 7% and have a dendritic field diameter of 282 ± 65 μm. These cells resemble cluster 9 of Badea and Nathans, but the cells shown by them vary in dendritic density.

Cluster 9 cells stratify at 45%; have a density of 0.05 $\mu m/\mu m^2$ and a dendritic field diameter of 326 μm (Fig. 13). Besides stratifying at a different level and being a little larger, these cells look very similar to the cells in cluster 8. Cluster 9 cells are similar to Sun et al.'s RG_{C3} cells. RG_{C3}

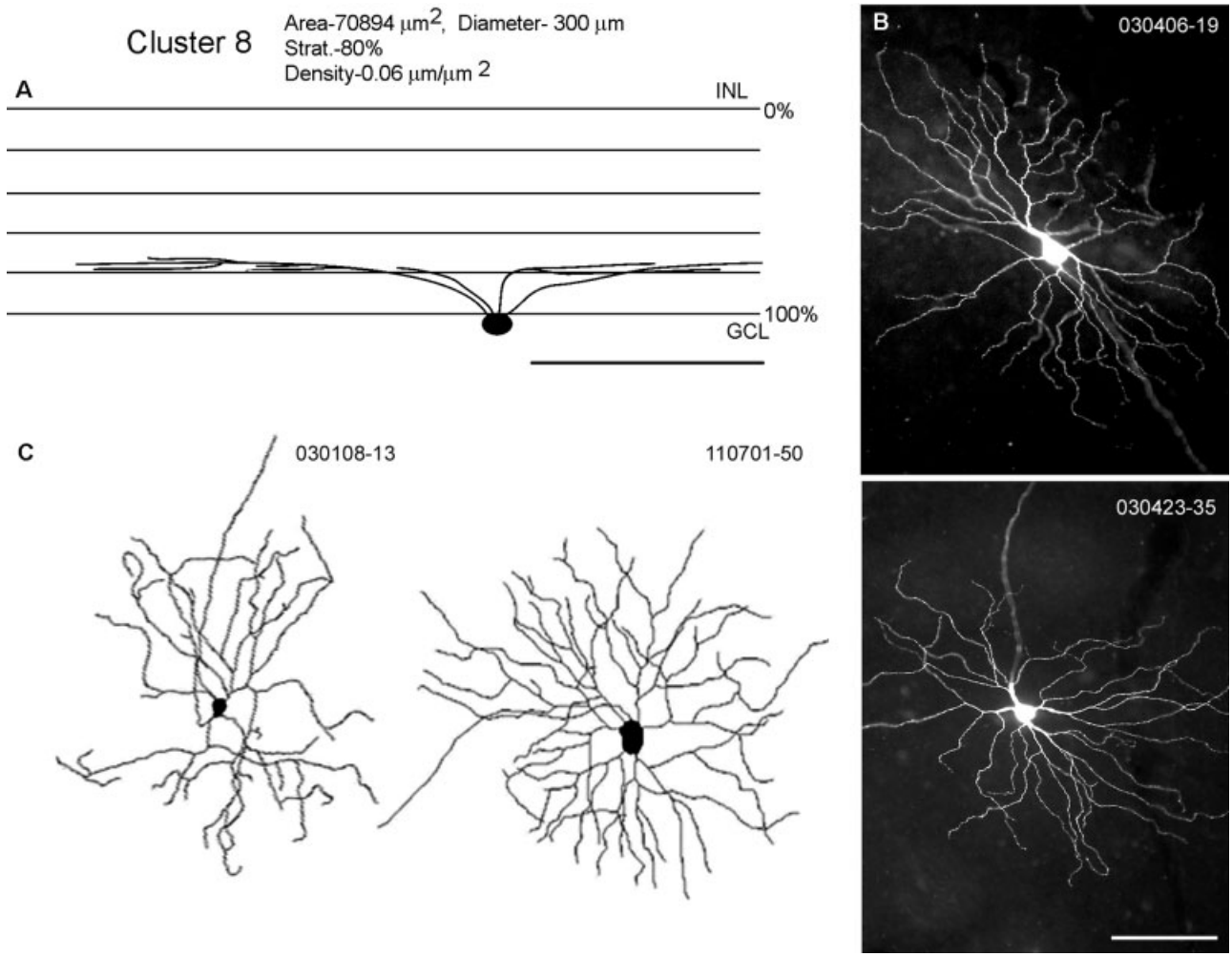

Fig. 12. Cells included in cluster 8. Conventions as in Figure 5.

cells stratify at 68±16% and have dendritic field diameter of 296 ±107 μm.

Cluster 10 cells stratify at 20%; have a density of 0.06 and a dendritic field diameter of 354 μm (Fig. 14). These large cells have 5–6 primary dendrites. To the eye, these cells look similar to the cells in clusters 8 and 9. In addition to stratifying at a different level and being much larger, the dendrites in this group typically have much longer terminal segments (+1.75 SD) than clusters 8 and 9. Cluster 10 cells look similar to Sun et al.'s RG_{C2} (inner) cells, which stratify at 32 ± 18% and have a dendritic field diameter of 283 ± 63 μm.

Cluster 11 cells stratify at 76%, have a density of 0.05, and a dendritic field diameter of 380 μm (Fig. 15). These are the largest cells we saw. They have 5–6 primary dendrites that radiate out from the cell body, branching at regular intervals and at fairly similar angles, resulting in an even dendritic field. Cluster 11 cells are similar to Sun et al.'s RG_{A1} cells. RG_{A1} cells stratify at 73 ± 9% and have a dendritic field diameter of 318 ± 74 μm. Cluster 10 and cluster 11 appear to be a paramorphic pair, evidently the On and Off alpha cells (Peichl et al., 1987).

Known cell types not included in this clustering

Bistratified cells were observed. The bistratified cells that we saw were clearly identical to those illustrated by Sun et al. (2002), and by Badea and Nathans (2004), and identified as probable directionally selective neurons. However, they were not included in the formal analysis. The reason was that the digital determination of the depth and thickness of stratification was unable to resolve two closely spaced dendritic arbors. This is not due to inadequate optical resolution in the z-dimension, but instead to tissue variability. If, for example, the tissue was less than perfectly flat, the two levels of arborization were measured as a single broad one. Such irregularities can effortlessly be compensated by a human observer, but judging depth "by eye" (Badea and Nathans, 2004) seemed to violate a fundamental premise of the exercise.

Another known type of ganglion cell is the sparse, wide-field type that expresses the light-sensitive protein, melanopsin (Hattar et al., 2002; Lin et al., 2004). These cells can be stained as a population by antibodies against mela-

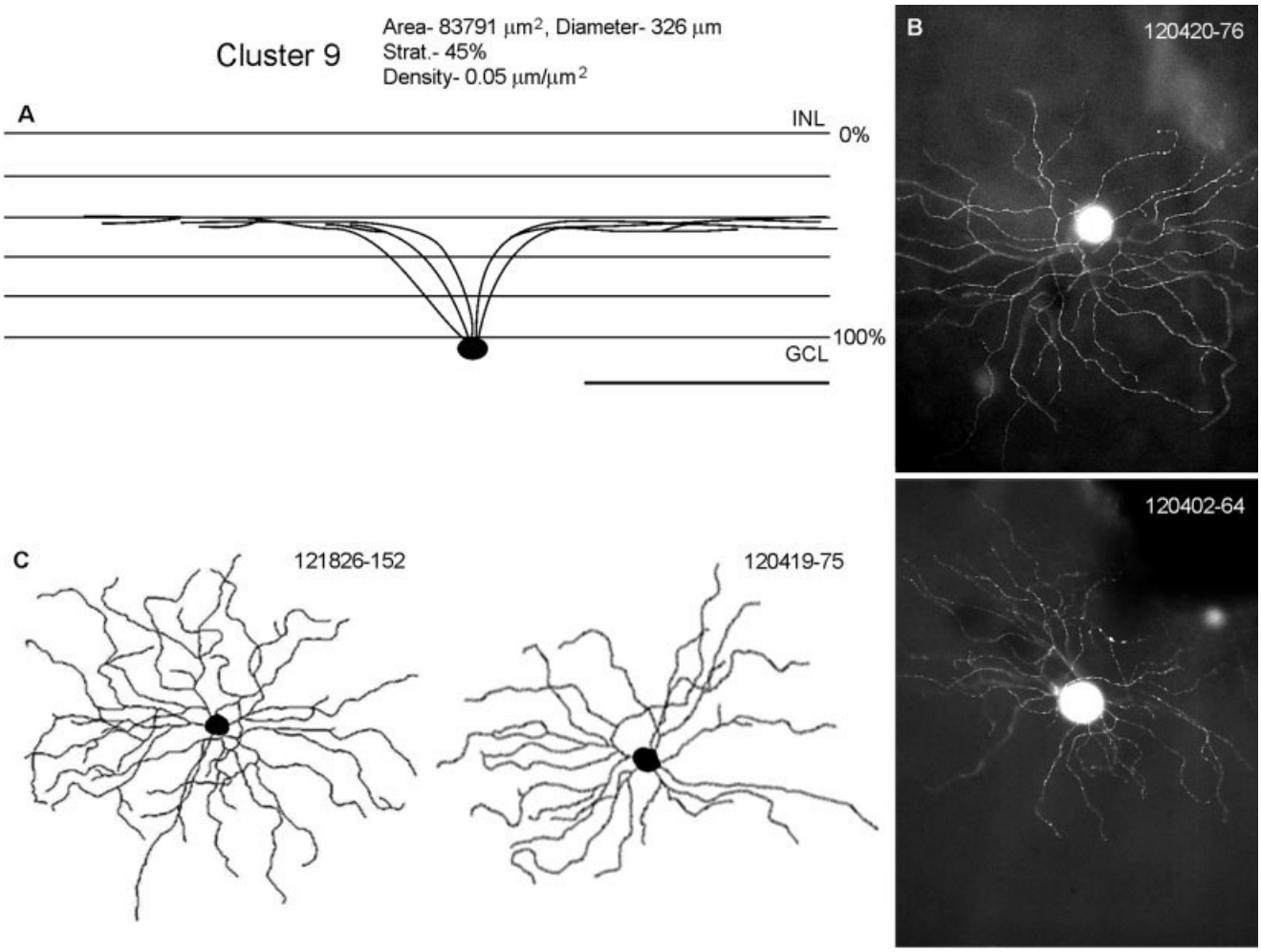

Fig. 13. Cells included in cluster 9. Conventions as in Figure 5.

nopsin; they make up about 1% of all ganglion cells in the mouse and thus would have been too sparse to form a cluster under our constraints. Indeed, two cells with the distinctive dendritic pattern of the melanopsin cells were observed in our sample of 219 cells. Our automated methods were unable to correctly describe their dendritic stratification; they were sorted by k means into clusters 8 and 11, with their wide dendritic fields as a primary influence.

DISCUSSION

Here we have described 11 morphological clusters of mouse ganglion cell, representing what would usually be termed cell types. The addition of a bistratified cell, which for trivial reasons we could not analyze, and the rare melanopsin cell makes a total of 13 putative ganglion cell types in the mouse retina. How complete a listing is this? The original sample from which the quantitatively analyzed cells were drawn was fairly large, and the cells were filled by three mechanistically independent techniques: microinjection, gene-gunning of DiI, or expression of GFP. The three methods have different biases and the group of cells seems statistically large enough to have included examples of most of the mouse retina's major cell types

How clearly could the cells be distinguished? From the outset it was clear that classifying the ganglion cells of the mouse retina was a difficult task: it is immediately evident that ganglion cells of the mouse are not as distinctive, one from the other, as are ganglion cells in the monkey, cat, or rabbit (Roska and Werblin, 2001; O'Brien et al., 2002; Rockhill et al., 2002; Dacey et al., 2003). However, there is some reason to think that the separation of the cells into groups did succeed. Many are readily mapped onto groupings identified by others (Fig. 16) (Sun et al., 2002; Badea and Nathans, 2004). Most meet Rodieck and Brening's (1983) criterion of coherent clusters (Fig. 3). It is worth noting that this coherence would not have been true in a two-parameter sort (Fig. 2). It is only with the addition of a third dimension that spaces between all the clusters become evident.

It is less certain that these are the definitive, terminal classifications of the cells. Within the clusters there is still variation in morphology and the fact that reliable separation of clusters has been achieved does not mean that a

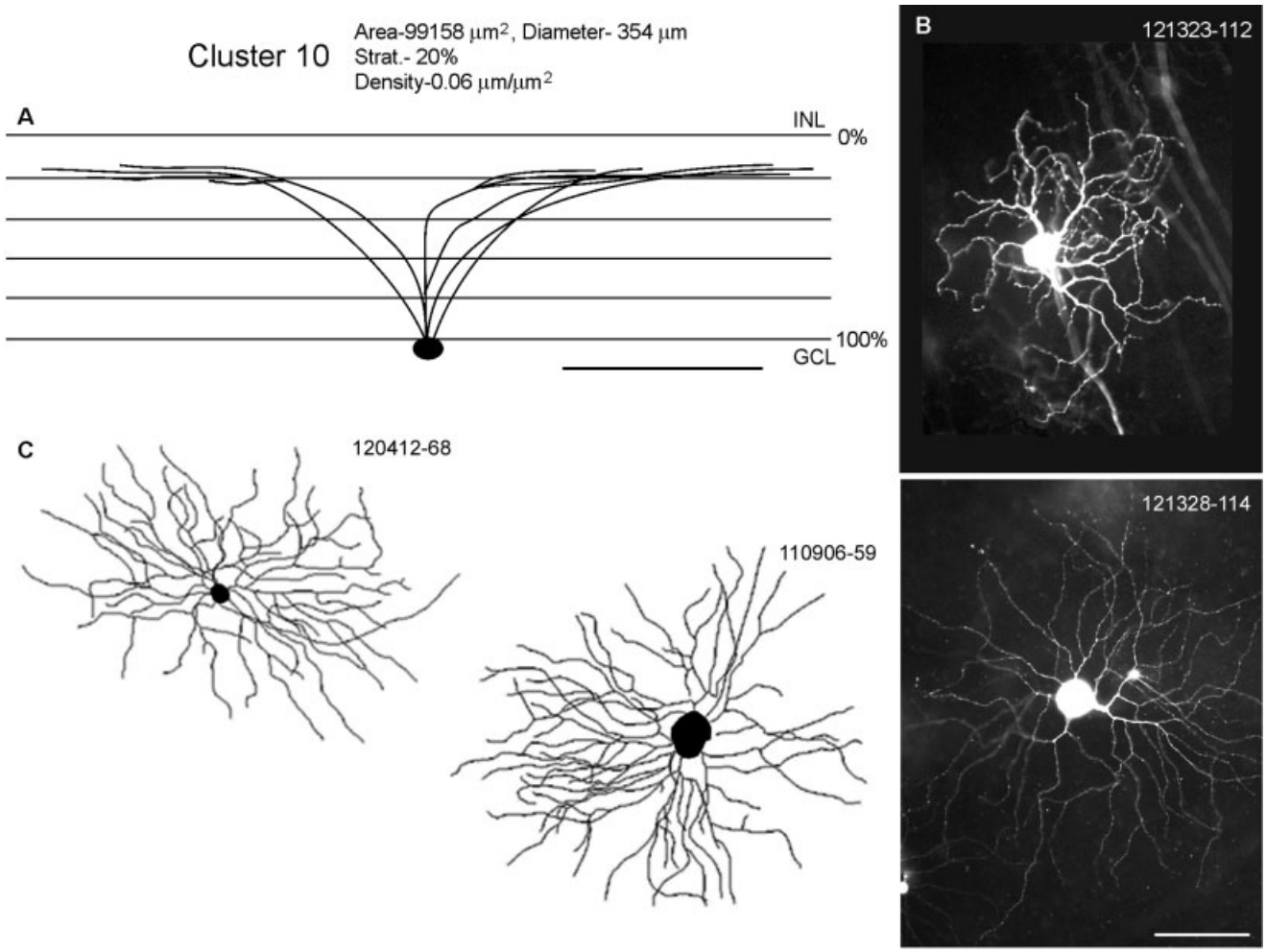

Fig. 14. Cells included in cluster 10. Conventions as in Figure 5.

finer separation utilizing additional morphological variables is not possible. One rare but clearly defined cell type, the melanopsin cell (Hattar et al., 2002; Lin et al., 2004), is known to have been excluded from the clustering (see Results).

A second kind of problem is represented by clusters 8 and 11, both of which are made up of large ganglion cells stratifying in the On sublayer. Which cells in these groups should be considered the homolog of On alpha cells (Peichl and Boycott, 1987)? Presumably the larger of the two, but without more information—notably, recording followed by microinjection—this cannot be concluded with certainty, and it is unwise to assume that any large ganglion cell encountered in the mouse (or any species other than the rabbit or cat) is by definition an alpha cell. Indeed, the ganglion cells of the mouse offer few obvious homologs with those of other mammals. Although tentative comparisons are possible in a few cases, as for alpha cells, most ganglion cell types have such weak correspondences that it is not clear how much value the exercise would have. When detailed correlation of physiology and morphology is available (Roska and Werblin, 2001), it will be possible to more precisely compare the ganglion cells of the mouse with those of other mammals; before then, such comparisons are likely to be futile.

What is learned about neuronal classification?

Given software that will measure many parameters, we were able to attempt different ways of sorting the cells. Our naïve initial assumption was that more information would automatically define the cells better—that a sorting based on many parameters would be better than one based on few parameters. This turned out not to be true (Fish, 2003). First, many of the parameters beloved of anatomists (branch angle, segment length, etc.) turn out to be highly correlated with each other (Table 1). For obvious reasons, this redundancy reduces the power of additional parameters. Less obvious is the fact that adding parameters actively degrades the classification; although the true parameters are correlated, the experimental noise sometimes is not. This means that excess parameters add little power but much variability and potential error to the analysis.

A vivid lesson was the extent to which selection of parameters can bias the final clustering. The important

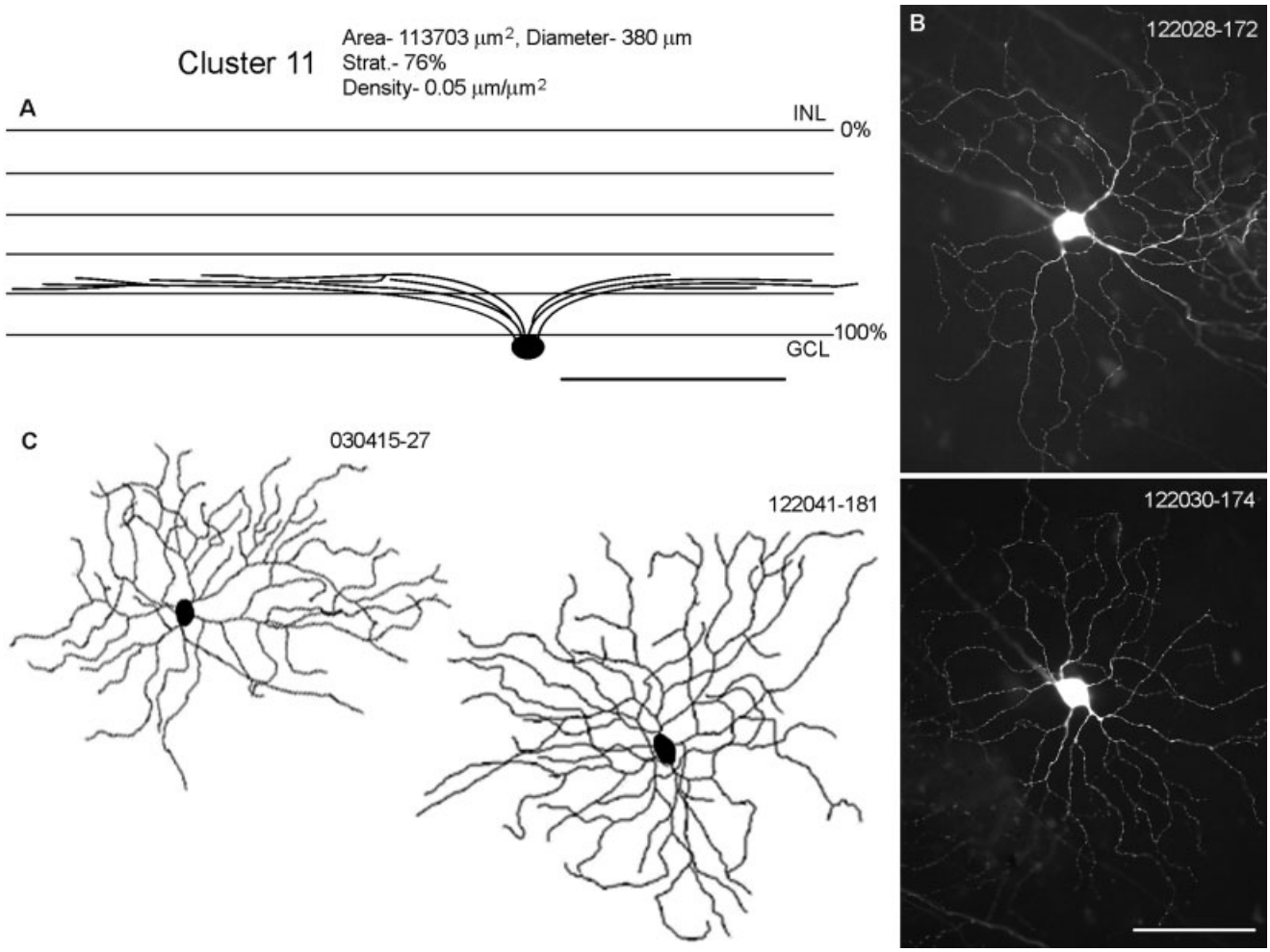

Fig. 15. Cells included in cluster 11. Conventions as in Figure 5.

point here is that an automated classification is not necessarily unbiased. In our view, asymmetry of the dendritic arbor is such a variable. We encountered retinal ganglion cells with asymmetric dendritic arbors, which are immediately striking and tempt one to classify them as a separate neuronal type, as has been done by others (Sun et al., 2002; Badea and Nathans, 2004). If one adds a parameter of dendritic symmetry with respect to the cell body, all of our clustering algorithms immediately create an asymmetric ganglion cell "type," because this parameter dominates. A series of such cells is shown in Figure 17. However, we believe that these are developmental accidents. First, their dendritic morphology is strikingly variable, some of the asymmetric cells having long, straight dendrites, others having recurving ones. Second, the asymmetric cells have widely divergent dendritic field size, some being small and some being large. Dendritic coverage area is a parameter of known physiological significance, as it directly controls the size of the ganglion cell's receptive field: it should trump asymmetry, which has unknown significance. Third, the asymmetric cells stratify at several different depths within the inner plexiform layer. Since depth controls the set of presynaptic inputs onto a ganglion cell, this necessarily means that the cells have differing connectivities. Given these differences, one would have to assume that each of the cells forms a distinct physiological class and therefore should at least tile the retinal surface. However, the frequency with which the cells were encountered was far too low to create the required series of four or five separate tilings, one for each size and level of stratification of the putative asymmetric-type ganglion cell. This undersampling is a cardinal feature of developmental variants, which seem to occur for all cell types (Wässle and Boycott, 1991; Masland et al., 1993).

Badea and Nathans (2004) included some asymmetric cells in conventional monostratified clusters, as we have done here (their figs. 13 and 14), but one group of asymmetric cells was defined by them as a type (their cluster 6). However, the clustering depended primarily on defining the inner arbor of the asymmetric cells as lying at 0% of the inner plexiform layer, a measurement that identifies the most proximal dendrites, at their exit from the soma, as part of the "arbor." By this definition all ganglion cells would have inner arbors at 0%. A larger sample of cells filled by their method would help resolve the issue, as

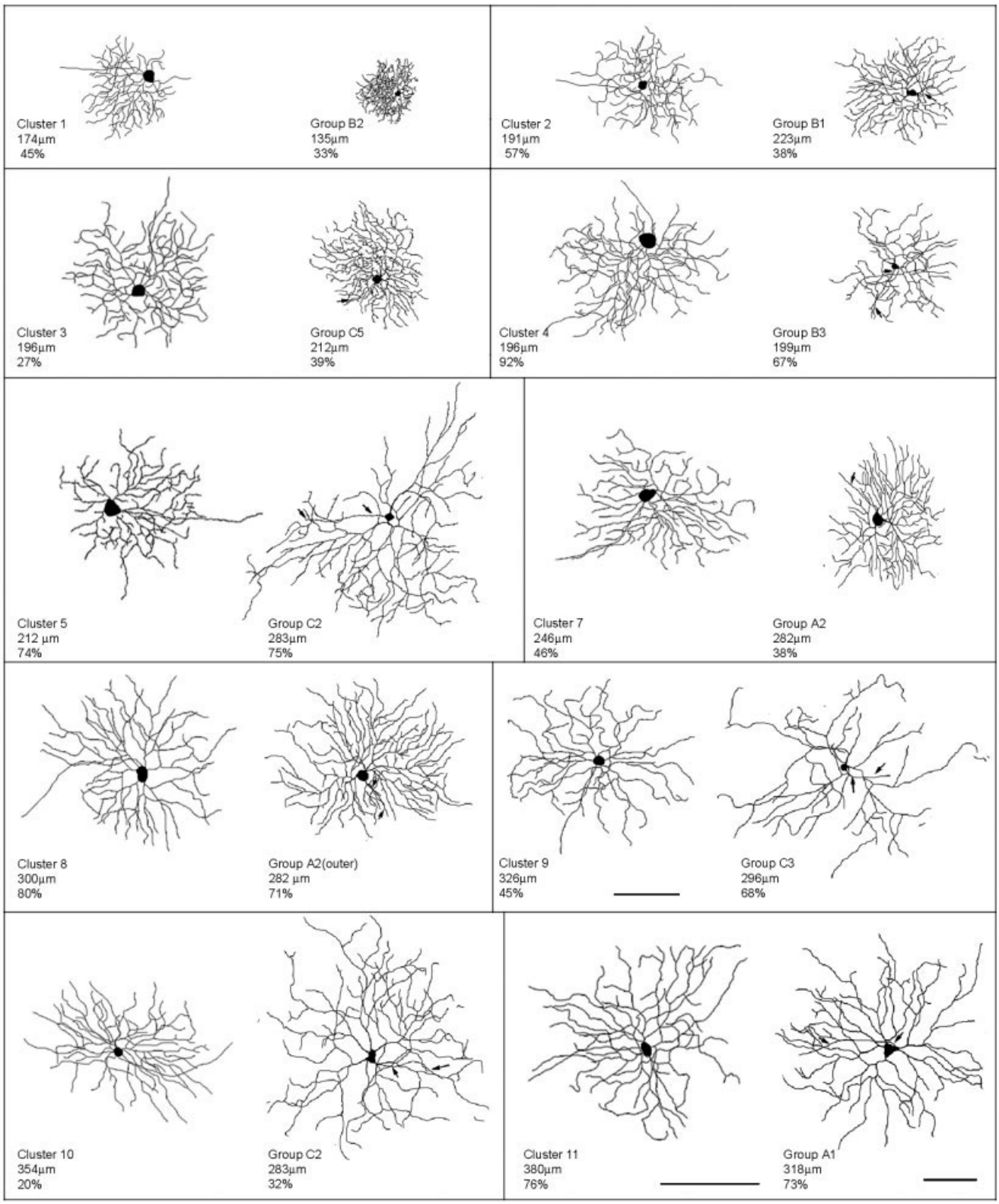

Fig. 16. Comparison of the unsupervised clusters with cell types distinguished by Sun et al. (2002), shown to the right of the clustered cells together with the group name assigned by them. Cells similar to those clustered by our methods were observed by Sun et al. Note, however, that the cells shown here include all of our clusters but do not include all of the cell types created by Sun et al. Scale bars = 100 µm.

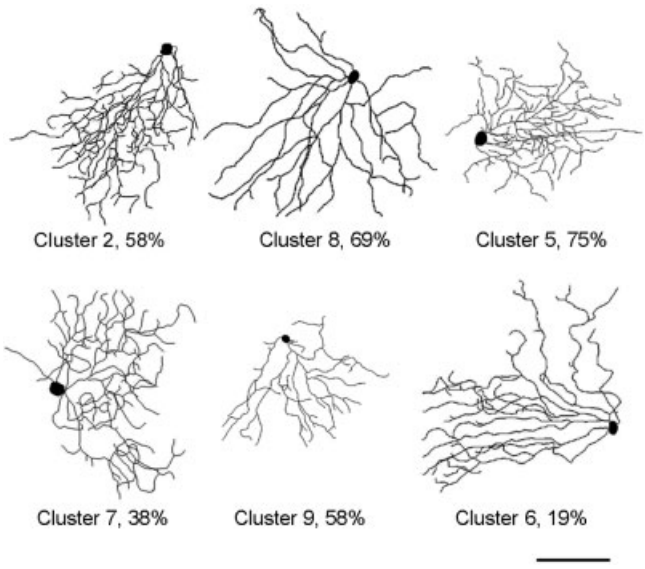

Fig. 17. Examples of asymmetric cells. These cells are robustly defined as forming their own cluster (i.e., a separate cell type) if a parameter measuring the asymmetry of the dendritic field asymmetry is used. The parameter of dendritic field asymmetry is generally so powerful that a cluster of asymmetric cells invariably results. However, the cells contained in such a cluster vary widely in other parameters, including those known to be of paramount physiological significance. For that reason the asymmetric cells shown here were assigned to various other clusters by our methods. The illustration shows, for each cell, the cluster number and the level of stratification within the inner plexiform layer. Scale bar = 100 μm.

would a better way to measure depth of stratification (see below).

How can formal classification be improved?

Two of the three parameters that we found useful are measures with a clearly known physiological consequence: depth within the IPL and dendritic field size, which directly reflect synaptic inputs and receptive field size, respectively. Dendritic field size is not difficult to measure precisely, but depth is much harder. Part of the reason is optical, as the z-axis is less well resolved by microscopy than x and y. Another problem is lack of flatness of the tissue, which is effortlessly compensated by a human observer, but which adds variability to an automated measurement. Most important, though, is a lack of basis of reference, as the edges of the inner plexiform layer have a variable structure and the cell soma is variably placed within the ganglion cell layer. This would be much improved by the use of fiducial marks, such as the bands of labeling created by the starburst cells (Tauchi and Masland, 1984; Keyser et al., 2000). (A convenient approach would be to use a transgenic animal in which the starburst cells express GFP.) The usefulness of improved depth measurement should not be underestimated. It now appears that the inner plexiform layer contains 10–15 substrata, each rigidly defined by the cells that participate in it (Vaney, 1991; Brown and Masland, 1999; Massey et al., 1999). With fiducial marks, it would be possible to improve the resolution of the measurement along this critical axis.

A second advance would be fully automated entry of the cell morphology into a digital representation. Aside from limiting the size of the sample that can be studied, manual entry introduces inevitable errors and simplifications. For example, we chose not to represent dendritic taper because the labor would have been prohibitive when a large sample of cells is also required. A second feature that was neglected is the presence of swellings or varicosities on the dendrites, which are known to distinguish certain cell types (i.e., melanopsin cells) from others. Fully automated entry, however, requires that the original morphological material be of very high contrast and exceptionally uniform strength of labeling. Also, the cells must appear on an exceptionally clean background (because of the segmentation problem). Even cells filled to a high current standard rarely meet all of these requirements.

Finally, more sophisticated clustering algorithms are almost certainly required. Techniques for unsupervised clustering are still in a developmental stage, particularly on the crucial issue of the assessing the proper number of clusters. It is now clear that a human observer uses very sophisticated means of visual pattern recognition, techniques that are not yet well understood and that automated routines struggle to reproduce (Sinha, 2002). For example, humans can with ease recognize thousands of human faces—a task not yet well accomplished by any unsupervised system. The power of human pattern recognition is quite evident when recognizing the shapes of neurons. Among other things, it is clear that the human observer carries out a highly nonlinear weighting of parameters. Dendritic taper, for example, may be important for distinguishing one type of neuron and unimportant in distinguishing another, may be weighted heavily if the cell also has varicosities, and weighted lightly if the cell does not. Sometimes these weightings are conscious; they have been the basis of anatomical descriptions for nearly a century. Often they are unconscious, and making them explicit should be a future goal.

LITERATURE CITED

Badea TC, Nathans J. 2004. Quantitative analysis of neuronal morphologies in the mouse retina visualized by using a genetically directed reporter. J Comp Neurol 480:331–351.

Brown SP, Masland RH. 1999. Costratification of a population of bipolar cells with the direction selective circuitry of the rabbit retina. J Comp Neurol 408:97–106.

Dacey DM, Peterson BB, Gamlin PD, Robinson FR. 2003. Fireworks in the primate retina: in vitro photodynamics reveals diverse LGN-projecting ganglion cell types. Neuron 37:15–27.

Doi M, Uji Y, Yamamura H. 1995. Morphological classification of retinal ganglion cells in mice. J Comp Neurol 356:368–386.

Feng G, Mellor RH, Bernstein M, Keller-Peck C, Nguyen QT, Wallace M, Nerbonne JM, Lichtman JW, Sanes JR. 2000. Imaging neuronal subsets in transgenic mice expressing multiple spectral variants of GFP. Neuron 28:41–51.

Fish D. 2004. Unsupervised parametric classification of mouse retinal ganglion cells. PhD Thesis, Harvard University, Department of Biology.

Gan W-B, Grutzendler J, Wong WT, Wong ROL, Lichtman JW. 2000. Multicolor "DiOlistic" labeling of the nervous system using lipophilic dye combinations. Neuron 27:219–225.

Ghosh K, Bujan S, Haverkamp S, Feigenspan A, Wässle H. 2004. Types of bipolar cells in the mouse retina. J Comp Neurol 469:70–82.

Gustincich S, Feigenspan A, Wu DK, Koopman LJ, Raviola E. 1997. Control of dopamine release in the retina: a transgenic approach to neural networks. Neuron 18:723–736.

Gustincich S, Feigenspan A, Sieghart W, Raviola E. 1999. Composition of the $GABA_A$ receptors of retinal dopaminergic neurons. J Neurosci 19:7812–7822.

Hattar S, Liao H-W, Takao M, Berson DM, Yau K-W. 2002. Melanopsin-

containing retinal ganglion cells: architecture, projections, and intrinsic photosensitivity. Science 295:1065–1070.

Jeon C-J, Strettoi E, Masland RH. 1998. The major cell populations of the mouse retina. J Neurosci 18: 8936–8946.

Kaufman L, Rousseeuw PJ. 1990. Finding groups in data: an introduction to cluster analysis. New York: John Wiley & Sons.

Keyser KT, MacNeil MA, Dmitrieva N, Wang F, Masland RH. 2000. Amacrine, ganglion, and displaced amacrine cells in the rabbit retina express nicotinic acetylcholine receptors. Vis Neurosci 17:743–752.

Lin B, Wang SW, Masland RH. 2004. Retinal ganglion cell type, size, and spacing can be specified independent of homotypic dendritic contacts. Neuron 43:475–485.

MacNeil MA, Masland RH. 1998. Extreme diversity among amacrine cells: implications for function. Neuron 20:971–982.

MacNeil MA, Heussy JK, Dacheux R, Raviola E, Masland RH. 1999. The shapes and numbers of amacrine cells: matching of photofilled with Golgi-stained cells in the rabbit retina and comparison with other mammalian species. J Comp Neurol 413:305–326.

Masland RH, Raviola E. 2000. Confronting complexity: strategies for understanding the microcircuitry of the retina. Annu Rev Neurosci 23: 249–284.

Masland RH, Rizzo JF III, Sandell JH. 1993. Developmental variation in the structure of the retina. J Neurosci 13:5194–5202.

Massey SC, Liu S, Zhang J, Li W. 1999. Confocal analysis of the rod pathway in the rabbit retina: connections with the matrix of indoleamine accumulating amacrine cells. Invest Ophthalmol Vis Sci Abstr 40:S437.

O'Brien BJ, Isayama T, Richardson R, Berson DM. 2002. Intrinsic physiological properties of cat retinal ganglion cells. J Physiol 538.3:787–802.

Peichl L, Ott H, Boycott BB. 1987. Alpha ganglion cells in mammalian retinae. Proc R Soc Lond B Biol 231:169–197.

Pignatelli V, Strettoi E. 2004. Bipolar cells of the mouse retina: a gene gun, morphological study. J Comp Neurol 476:254–266.

Rockhill RL, Euler T, Masland RH. 2000. Spatial order within but not between types of retinal neurons. Proc Natl Acad Sci U S A 97:2303–2307.

Rockhill RL, Daly F, MacNeil MA, Brown SP, Masland RH. 2002. The diversity of ganglion cells in a mammalian retina. J Neurosci 22:3831–3843.

Rodieck RW, Brening RK. 1983. Retinal ganglion cells: properties, types, genera, pathways and trans-species comparisons. Brain Behav Evol 23:121–164.

Roska B, Werblin F. 2001. Vertical interactions across ten parallel, stacked representations in the mammalian retina. Nature 410:583–587.

Sinha P. 2002. Recognizing complex patterns. Nat Neurosci 5:1093–1097.

Sun W, Li N, He S-G. 2002. Large-scale morphological survey of mouse retinal ganglion cells. J Comp Neurol 451:115–126.

Tauchi M, Masland RH. 1984. The shape and arrangement of the cholinergic neurons in the rabbit retina. Proc R Soc Lond B Biol 223:101–119.

Tauchi M, Masland RH. 1985. Local order among the dendrites of an amacrine cell population. J Neurosci 5:2494–2501.

Vaney DI. 1991. The mosaic of amacrine cells in the mammalian retina. Prog Retinal Res 9:49–100.

Wässle H, Boycott BB. 1991. Functional architecture of the mammalian retina. Physiol Rev 71:447–480.

Wässle H, Peichl L, Boycott BB. 1981. Dendritic territories of cat retinal ganglion cells. Nature 292:344–345.